

Article

Retrieval of Chlorophyll a Concentration Using GOCI Data in Sediment-Laden Turbid Waters of Hangzhou Bay and Adjacent Coastal Waters

Yixin Yang¹, Shuangyan He^{1,2,3,*}, Yanzhen Gu^{1,2}, Chengyue Zhu⁴, Longhua Wang¹, Xiao Ma^{3,5}
and Peiliang Li^{1,2}

¹ Ocean College, Zhejiang University, Zhoushan 316021, China; zjursyx@zju.edu.cn (Y.Y.);

guyanzhen@zju.edu.cn (Y.G.); 3180102137@zju.edu.cn (L.W.); lipeiliang@zju.edu.cn (P.L.)

² Hainan Institute, Zhejiang University, Sanya 572025, China

³ State Key Laboratory of Satellite Ocean Environment Dynamics, Second Institute of Oceanography, Ministry of Natural Resources, Hangzhou 310012, China; maxiao@sio.org.cn

⁴ Shanghai Marine Monitoring and Forecasting Center, Shanghai 200050, China; zcy19921201@gmail.com

⁵ Observation and Research Station of Yangtze River Delta Marine Ecosystems, Ministry of Natural Resources, Zhoushan 316022, China

* Correspondence: hesy@zju.edu.cn

Abstract: The Geostationary Ocean Color Imager (GOCI) provided images at hourly intervals up to 8 times per day with a spatial resolution of 500 m from 2011 to 2021. However, in the typical sediment-laden turbid water of Hangzhou Bay, valid ocean color parameters in operational data products have been extensively missing due to failures in atmospheric correction (AC) and bio-optical retrieval procedures. In this study, the seasonal variations in chlorophyll a (Chl-a) concentrations in Hangzhou Bay derived using GOCI data in 2020 were presented. First, valid remote sensing reflectance data were obtained by transferring neighboring aerosol properties of less to more turbid water pixels. Then, we improved a regionally empirical Chl-a retrieval algorithm in extremely turbid waters using GOCI-derived surface reflectance and field Chl-a measurements and proposed a combined Chl-a retrieval scheme for both moderately and extremely turbid water in Hangzhou Bay. Finally, the seasonal variation in Chl-a was obtained by the GOCI, which was better than operational products and in good agreement with the buoy data. The method in this study can be effectively applied to the inversion of Chl-a concentration in Hangzhou Bay and adjacent sea areas. We also presented its seasonal variations, offering insight into the spatial and seasonal variation of Chl-a in Hangzhou Bay using the GOCI.

Keywords: GOCI; atmospheric correction; turbid water; chlorophyll a; Hangzhou Bay



Citation: Yang, Y.; He, S.; Gu, Y.; Zhu, C.; Wang, L.; Ma, X.; Li, P. Retrieval of Chlorophyll a Concentration Using GOCI Data in Sediment-Laden Turbid Waters of Hangzhou Bay and Adjacent Coastal Waters. *J. Mar. Sci. Eng.* **2023**, *11*, 1098. <https://doi.org/10.3390/jmse11061098>

Academic Editors: Yuji Sakuno, Mitsuhiro Toratani and Hiroto Higa

Received: 26 March 2023

Revised: 18 May 2023

Accepted: 19 May 2023

Published: 23 May 2023



Copyright: © 2023 by the authors. Licensee MDPI, Basel, Switzerland. This article is an open access article distributed under the terms and conditions of the Creative Commons Attribution (CC BY) license (<https://creativecommons.org/licenses/by/4.0/>).

1. Introduction

Phytoplankton play a key role in the marine biogeochemical cycle and global carbon dynamics [1] and largely control the productivity of coastal ecosystems. The chlorophyll a (Chl-a) concentration has been widely used as an index of phytoplankton abundance to reflect the productivity and trophic conditions of estuaries and coastal and oceanic waters [2,3]. The change in Chl-a concentration is affected by climate and environmental factors, such as temperature, nutrients, rainfall, ocean currents, river inflow, and turbidity [4,5]. Monitoring the dynamics of Chl-a is of great interest and importance for biogeochemical researchers.

Water color remote sensing technology can observe the ocean synchronously over a large range, which is an important technical means for water research. The Chl-a concentration and primary production in oceanic waters can be estimated using data from spaceborne ocean-color sensors [6]. Compared with ocean color sensors (e.g., the Sea-viewing Wide Field-of-view Sensor (SeaWiFS) and the Moderate Resolution Imaging Spectroradiometer

(MODIS)) onboard polar-orbiting satellites, geostationary satellites are capable of a high revisit frequency, and their high temporal sampling capacity can greatly enhance our ability to monitor and assess coastal ocean dynamics [7]. The world's first geostationary spaceborne ocean color sensor launched by South Korea, the Geostationary Ocean Color Imager (GOCI), was in orbit from 2010 to 2021. It acquired data with a high spatial resolution (500 m) and a high temporal resolution (1 h, eight images per day) and was uniquely capable of monitoring short-term and regional oceanic phenomena (e.g., tide dynamics, red tides, river plumes, and sediment transport) [8].

Although operational satellite water color data of Chl-a concentrations in the open ocean have been proven to be reliable and useful, the quality of satellite data products often deteriorates in coastal waters, such as in Hangzhou Bay, where the operational atmospheric correction procedure and bio-optical retrieval algorithms often fail due to its sediment-laden highly turbid waters. This leads to few available valid Chl-a pixels in operational ocean color data products distributed by NASA's Ocean Biology Processing Group (OBPG) and the Korea Ocean Satellite Center (KOSC) in Hangzhou Bay. Many efforts have been made to improve the accuracy of atmospheric correction and establish regional retrieval algorithms for Chl-a in various coastal waters.

To improve the atmospheric correction performance in turbid waters, several methods have been proposed. For example, Hu et al. [9] proposed a "nearest neighbor" method, which assumes that aerosol types do not vary much on a spatial scale of approximately 50–100 km, and the aerosol type of adjacent less turbid water pixels can be transferred to turbid water pixels, thus solving the problem of negative water-leaving radiance values in turbid water. Wang and Shi [10] proposed using two shortwave infrared (SWIR) bands rather than two traditional near-infrared bands (NIR) in atmospheric correction processing for highly turbid water by taking advantage of the fact that the absorption capacity of water bodies in the shortwave infrared band is stronger than that in the near-infrared band. This algorithm has been applied well using MODIS data and has been widely used in various coastal waters worldwide [11]. He et al. [12] proposed using the alternative ultraviolet wavelength for turbid waters (UV-AC) based on the neglectable water-leaving radiance in the ultraviolet spectral range, and to avoid extrapolation error amplification with the increase in extrapolation spectral distance in the traditional atmospheric correction procedure, an interpolation-based UV-SWIR-AC algorithm for turbid waters using one ultraviolet and two shortwave infrared bands was further developed. Tian et al. [13] proposed a regional atmospheric correction method based on an artificial neural network (ANN) model, deriving the water-leaving reflectance using the GOCI in turbid coastal water areas of the Bohai Sea. Wang et al. [14] improved the atmospheric correction algorithm based on the Gordon and Wang [15] scheme by estimating remote-sensing reflectance in the near-infrared bands with artificial neural networks over turbid waters.

In terms of Chl-a retrieval algorithms, many methods have been developed for different water types. In Case I waters, the water optical properties are dominated by phytoplankton [16], and the quantitative retrieval methods of Chl-a concentrations are usually empirical ocean color (OC) algorithms (OC3, OC4, OC5, OC6) using maximum blue-green band ratios [17–19]. Note that the OC3 algorithm is used in operational Chl-a products from the GOCI by the KOSC. For Case II waters with complex water components, the correlation between Chl-a concentration and spectral reflectance ratio using red/near-infrared bands could be stronger than using blue and green bands in Case I waters [20], and many retrieval methods, including empirical and semianalytical algorithms, have been developed for various estuaries and coasts. Empirical studies are based on the relationship between local measured Chl-a and band ratios of the remote sensing reflectance for different ocean color sensors [21–24]. For example, Shen et al. [21] established an empirical relationship between a synthetic chlorophyll index (SCI) and Chl-a concentration by using field data in the Yangtze River Estuary and its adjacent waters and proposed an inversion algorithm for MERIS in the seasonal Chl-a estimation of turbid sediment-laden waters. Siswanto et al. [23] provided alternative empirical ocean color algorithms for SeaWiFS

in the Yellow and East China Seas. Such empirical algorithms are highly reliant on in situ datasets and are therefore usually only applicable in specific regions. Additionally, semianalytical algorithms, including spectral optimization methods, which are based on the relationship between Chl-a concentrations and water's inherent optical properties, have also been utilized. For example, Le et al. [25] proposed a four-band semianalytical algorithm to estimate chlorophyll a in the highly turbid water of Taihu Lake, China. Yi et al. [26] proposed a four-band quasi-analytical algorithm for MODIS in the turbid waters of the Yellow River Estuary, the Gulf of Mexico, and Chesapeake Bay. These algorithms, however, rely on varying bio-optical relationships in different coastal waters [27].

The water in Hangzhou Bay is extremely turbid and changes rapidly under the influence of strong tides, which has attracted widespread attention from researchers [28–30]. The GOCI has the advantage of monitoring dynamic environmental changes [31]; however, none of the Chl-a retrieval methods are tuned with high precision for the turbid waters of Hangzhou Bay. Moreover, we have observed that operational GOCI Chl-a products in Hangzhou Bay are usually missing. To obtain a more accurate estimation of Chl-a concentrations from GOCI data in Hangzhou Bay, we conducted atmospheric correction processing and developed an improved regional Chl-a concentration algorithm for highly turbid water. We also presented its seasonal variations, offering insight into the spatial and seasonal variation in Chl-a in Hangzhou Bay using the GOCI.

2. Data and Methods

2.1. Study Area

Hangzhou Bay is a bay in the Yangtze River delta region of the East China Sea, as shown in Figure 1, covering an area of approximately 5500 km². The average depth of its water is 6–10 m. It is a famous strong tidal estuary bay with an average daily tidal range of 3.5 m. The coastal waters of the Hangzhou Bay area are also affected by the northbound Taiwan warm current and the diluted water of the Yangtze River [32]. Approximately 470 million tons of sediment are transported from the Yangtze River to the outer seashore every year, which provides a rich source of sediments for Hangzhou Bay [33]. Its water is highly turbid, with sediment concentrations ranging from 0 to 5000 mg/L.

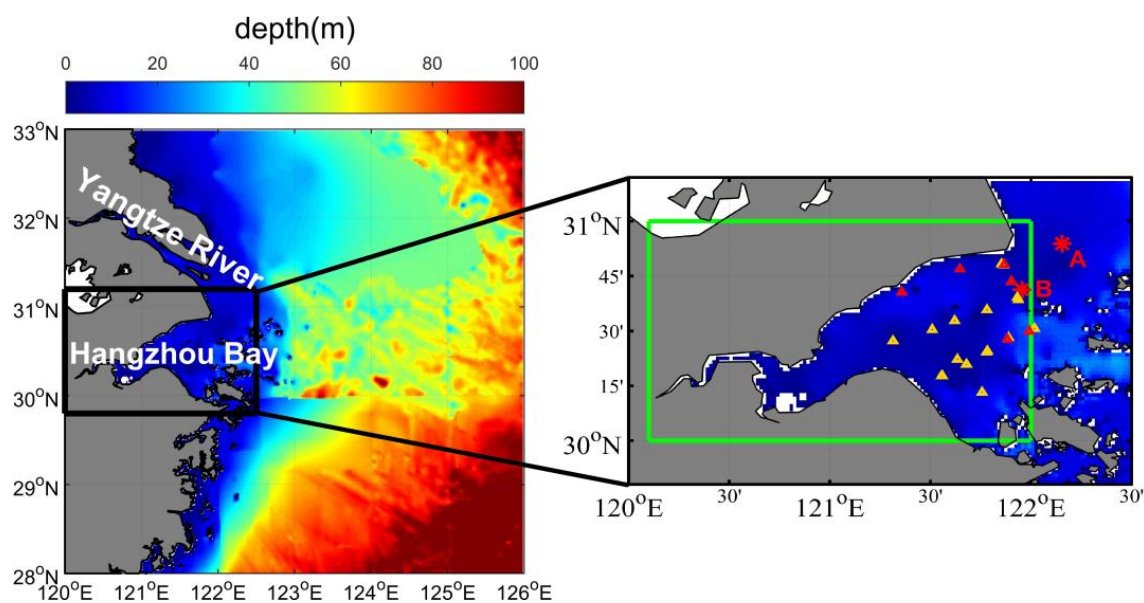


Figure 1. Location of the study area. Hangzhou Bay is indicated in a green rectangle. The two red stars (A and B) indicate the locations of the two buoys used in this study. The 26 triangles (in yellow and red) indicate site locations of cruises (6 match-up sites in red were used in this study). The background color represents the water depth.

2.2. Field Data

Two mooring buoys were deployed to monitor the ocean environment at the mouth of Hangzhou Bay (as shown in Figure 1) by the Shanghai Marine Monitoring and Forecasting Center. The data period of Buoy A is from 1 January 2020 to 31 December 2020, and that of Buoy B is from 1 February 2021 to 30 November 2021. The buoys were set to measure and transmit data hourly every day, and there are 24 in situ values per day. Each buoy is equipped with a multiparameter water quality sensor (YSI EXO2). The surface water salinity, temperature, turbidity, pH, Chl-a, and dissolved oxygen were synchronously measured per hour daily. Concerning the Chl-a levels used in this study, the measuring range of the instrument is 0 to 400 mg/m³, the resolution is 0.01 mg/m³, and the accuracy has been calibrated with a Rhodamine WT across the full range with an R² no less than 0.999 (<https://cdn.shopify.com/s/files/1/0065/4616/1748/files/YSI-EXO-Brochure.pdf?v=1667258816>, accessed on 10 May 2023). The Chl-a data collected during three cruises (August 2016, August 2017, August 2018) in Hangzhou Bay by the Observation and Research Station of Marine Ecosystem in the Yangtze River Estuary, Ministry of Natural Resources, were also used in this study. The Chl-a data at 26 stations (8 stations in August 2016, 7 stations in August 2017, and 11 stations in August 2018) were measured (triangles in Figure 1). During these cruises, an ECO Fluorometer of the Sea-Bird Scientific was used to collect Chl-a. The measuring range of the instrument for Chl-a is 0 to 125 mg/m³, the resolution is 0.025 mg/m³, and the accuracy has been calibrated with a Rhodamine WT across the full range with an R² no less than 0.999 (<https://www.seabird.com/product.detail-print.version.jsa?id=60429374754>, accessed on 10 May 2023). According to our calibration results using the standard Rhodamine WT (Chl-a of 0.0, 3.0, 30.0, and 300.0 mg/m³), the mean relative percentage error is within 2%. The waters in Hangzhou Bay and the adjacent coastal area are highly turbid, as illustrated in the RGB composite GOCI image in Figure 2a.

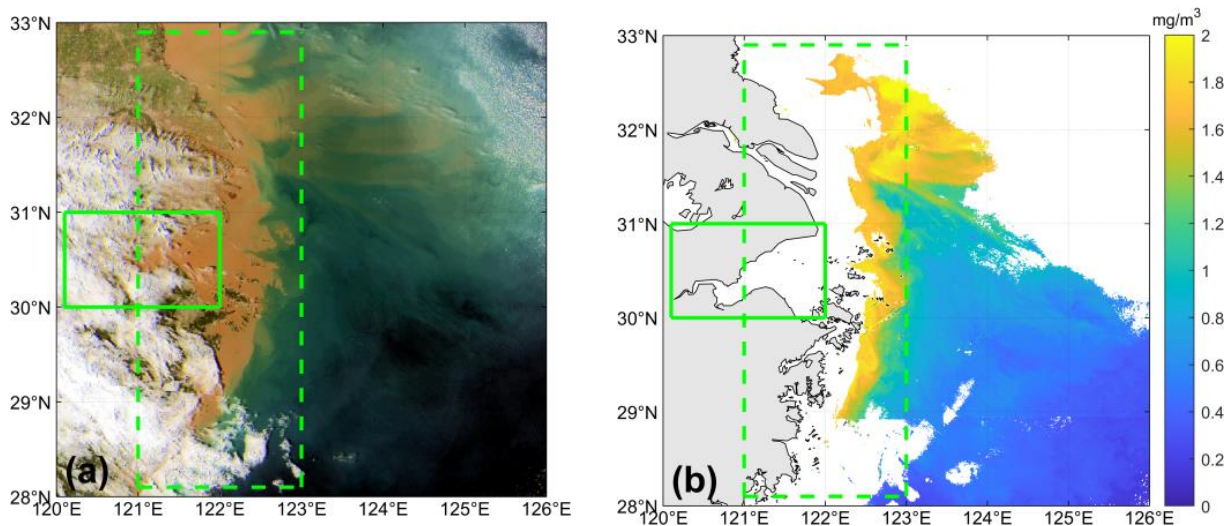


Figure 2. (a) RGB image composited from GOCI Rayleigh-corrected reflectance at 680, 555, and 443 nm at 05:16 (UTC) on 10 February 2020. (b) The corresponding chlorophyll a concentration retrieved by the OC3 algorithm using GDPS 2.0, and the white color represents no valid data. Hangzhou Bay is indicated by a green solid line rectangle, and the adjacent coastal waters are indicated by a green dashed rectangle.

2.3. GOCI Data

The GOCI has eight visible to near-infrared bands (412, 443, 490, 555, 660, 680, 745, and 865 nm). It acquires images 8 times per day in hourly intervals from 00:15 UTC to 07:45 UTC with a spatial resolution of approximately 500 m, and its observation area of 2500 km × 2500 km covers Korea, Japan, and the eastern coast of China [8].

The GOCI level 1b data during 2020 and 2021 were downloaded from the Ocean Color web at <https://oceandata.sci.gsfc.nasa.gov/> (accessed on 24 January 2022). Note that the time range of Buoy B is from February to November 2021, while the Chl-a product of the GOCI is only available until March 2021.

The Rayleigh-corrected reflectance at 8 spectral bands was processed from the level 1b files using the SeaWiFS Data Analysis System (SeaDAS) distributed by NASA’s Ocean Biology Processing Group (OBPG). The Chl-a data from the GOCI operational level 2 files were downloaded from the Korea Ocean Satellite Center (KOSC) website at <https://kosc.kiost.ac.kr/index.nm> (accessed on 24 January 2022), which was generated using the GOCI Data Processing System (GDPS) 2.0 distributed by the KOSC. As an example, an RGB image (Figure 2a) was composited from GOCI Rayleigh-corrected reflectance at 05:16 (UTC) on 10 February 2020, and the Chl-a concentration (Figure 2b) retrieved from OC3 algorithm using GDPS 2.0. It can be seen (Figure 2) that Chl-a data are missing for cloudless pixels in sediment-laden turbid waters of Hangzhou Bay (green solid-line rectangle) and adjacent coastal waters (green dashed-line rectangle).

2.4. Atmospheric Correction of GOCI Data

To obtain valid retrieval results for Chl-a concentration in the sediment-laden turbid waters of Hangzhou Bay and adjacent coastal areas, which may be missing from the operational data products, we used the cloud masking method for turbid water [34] in our atmospheric correction procedure, and the neighboring aerosol properties of less turbid water pixels were transferred to turbid water during the aerosol correction processing [9]. The steps we followed for our atmospheric correction procedure are outlined below.

2.4.1. Rayleigh Scattering Correction

The Rayleigh scattering corrected reflectance (ρ_{rc}) for all bands was first calculated as:

$$\rho_{rc}(\lambda) = \rho_t(\lambda) - \rho_r(\lambda) = \rho_a(\lambda) + t_v(\lambda) \times \rho_w(\lambda) \tag{1}$$

where ρ_t is the total reflectance at the top of the atmosphere as measured by the GOCI, ρ_r is the Rayleigh scattering reflectance by air molecules in the absence of aerosols, ρ_a is the aerosol scattering reflectance including the interactive scattering between air molecules and aerosol, ρ_w is the desired water-leaving reflectance, t_v is the diffuse transmission coefficient from the sea surface to the satellite sensor, and λ is the wavelength.

The definition of the reflectance in Equation (1) is:

$$\rho(\lambda) = \frac{\pi \times L(\lambda)}{F_0(\lambda) \times \cos \theta_0} \tag{2}$$

where L is the upwards radiance, F_0 is the extraterrestrial solar irradiance, and θ_0 is the solar zenith angle. ρ_r was derived from the GOCI level 1b data using SeaDAS.

2.4.2. Cloud Masking

The cloudy pixels were masked out using an improved method of Lu et al. [34] based on Nordkvist et al. [35] for turbid water as follows:

$$\rho_{rc}(412 \text{ nm}) > 0.07 \text{ and } \varepsilon_{max} < 2.5 \text{ and } \rho_{rc}(865 \text{ nm}) \geq 0.027 \tag{3}$$

$$\frac{\rho_{rc}(412 \text{ nm})}{\rho_{rc}(660 \text{ nm})} > 1 \text{ and } \varepsilon_{max} < 2.5 \text{ and } \rho_{rc}(865 \text{ nm}) \geq 0.027 \tag{4}$$

where $\varepsilon_{max} = \frac{MAX[\rho_{rc}(412 \text{ nm}), \rho_{rc}(660 \text{ nm}), \rho_{rc}(680 \text{ nm}), \rho_{rc}(865 \text{ nm})]}{MIN[\rho_{rc}(412 \text{ nm}), \rho_{rc}(660 \text{ nm}), \rho_{rc}(680 \text{ nm}), \rho_{rc}(865 \text{ nm})]}$.

2.4.3. Correction of Aerosol Contribution

The aerosol contribution was corrected according to Hu et al. [9]. Assuming that aerosol types vary little over relatively small spatial scales (~50–100 km), the aerosol types over less turbid water were first obtained and then transferred to the nearest neighboring turbid water area. In this study, by observing the GOCI-derived aerosol radiance (L_a) data in less turbid water in 2020, the ranges of L_a at different wavelengths over our study area, as shown in Table 1, are defined as reasonable values for nearby less turbid water pixels.

Table 1. Data range of L_a over less turbid water pixels near Hangzhou Bay.

Wavelength (nm)	L_a ($W \cdot m^2 \cdot sr^{-1}$)
412, 443	0~3
490, 555	0~4
660, 680, 745	0~4.5
865	0~3.5

Subtracting the aerosol contribution, we obtained the remote sensing reflectance (R_{rs}):

$$R_{rs}(\lambda) = \frac{L_w(\lambda)}{t_s(\lambda) \times \cos \theta_0 \times F_0(\lambda)} \tag{5}$$

where L_w is the water-leaving radiance and t_s is the diffuse transmission coefficient from the sun to the sea surface.

2.5. Related Chl-a Retrieval Algorithms

2.5.1. Regional Chl-a Retrieval Algorithm in Highly Turbid Water around Hangzhou Bay

Using MERIS data, Shen et al. [21] developed a retrieval algorithm for Chl-a based on a synthetic chlorophyll index (SCI), as shown in Equations (6)–(8), which was designed for turbid waters with high sediment concentrations in the Yangtze River Estuary:

$$H_{chl} = [R_{rs}(\lambda_4) + \frac{\lambda_4 - \lambda_3}{\lambda_4 - \lambda_2} \times (R_{rs}(\lambda_2) - R_{rs}(\lambda_4))] - R_{rs}(\lambda_3) \tag{6}$$

$$H_{\Delta} = R_{rs}(\lambda_2) - [R_{rs}(\lambda_4) + \frac{\lambda_4 - \lambda_2}{\lambda_4 - \lambda_1} \times (R_{rs}(\lambda_1) - R_{rs}(\lambda_4))] \tag{7}$$

$$SCI = H_{chl} - H_{\Delta} = 1.24R_{rs}(\lambda_4) - R_{rs}(\lambda_3) - 0.74R_{rs}(\lambda_2) + 0.5R_{rs}(\lambda_1) \tag{8}$$

where H_{chl} is a parameter relevant to chlorophyll pigments, H_{Δ} is a correction factor for H_{chl} in the presence of mid- or high-sediment loads, and λ represents the wavelength. The $\lambda_1 \sim \lambda_4$ are 560, 620, 665, and 681 nm, respectively.

2.5.2. The OC3 Algorithm Used in the GOCI Level 2 Operational Chl-a Data Product

The OC3 algorithm is used to generate the GOCI level 2 data product in GDPS version 2.0. The OC3 algorithm applicable in waters with low and moderate turbidity is shown in Equations (9) and (10).

$$\log_{10}[C_{Chl-a}] = c_0 + c_1 \log_{10} X + c_2 \log_{10}^2 X + c_3 \log_{10}^3 X + c_4 \log_{10}^4 X \tag{9}$$

$$X = \max(R_{rs}(443 \text{ nm}), R_{rs}(490 \text{ nm})) / R_{rs}(555 \text{ nm}) \tag{10}$$

The $c_0 \sim c_4$ values are 0.0831, −1.9941, 0.5629, 0.2944, and −0.5458, respectively, and they were obtained using a total of 130 field data points near the coastal Korean Peninsula [19].

2.5.3. Preprocessing for an Improved Chl-a Retrieval Algorithm in This Study

To improve the Chl-a retrieval algorithm in the highly turbid water of Hangzhou Bay, we first obtained the match-up dataset of GOCI-derived R_{rs} and field Chl-a. The time difference between the satellite data and the field Chl-a measurements of the buoy and cruises is within ± 30 min, and the GOCI R_{rs} were calculated using the arithmetic mean values of 3×3 pixels centered at the location of cruise sites and Buoys A and B to reduce the random noise effects of the satellite data. We obtained 159 match-up samples, with 26, 26, 44, and 63 samples in spring, summer, autumn, and winter, respectively. Thereinto, cruise data at 6 stations (4 stations in August 2017 and 2 stations in August 2018) were used (red triangles in Figure 1).

Using our 159 match-up data, the GOCI-derived R_{rs} data (at 555, 660, 680 nm) obtained using three windows of 1×1 , 3×3 , and 5×5 pixels were intercompared (Figure 3). The MAPE of R_{rs} values for the 1×1 versus 3×3 pixel window and the 3×3 versus 5×5 pixel window are smaller than those of the 1×1 versus 5×5 pixel window. This means that the 3×3 pixel window can reduce noise as well as the 5×5 pixel window, and the mean values of the 3×3 pixel window are closer to the 1×1 pixel values. Therefore, the 3×3 pixel window was selected to calculate the GOCI R_{rs} .

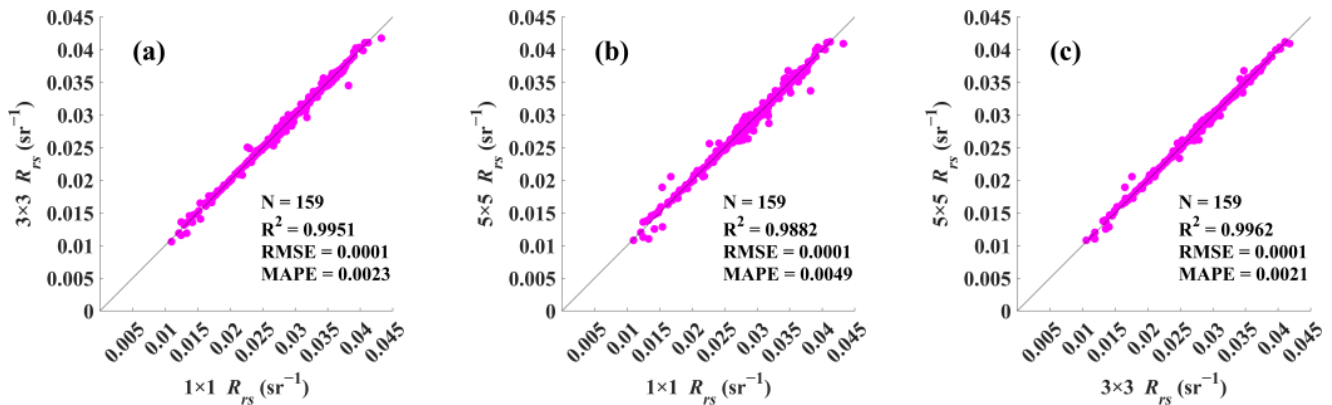


Figure 3. Comparison of GOCI spectral R_{rs} data (at 555, 660, 680 nm) obtained using three windows of 1×1 , 3×3 and 5×5 pixels. (a) R_{rs} values of the 1×1 vs. 3×3 pixel window. (b) R_{rs} values of the 1×1 vs. 5×5 pixel window. (c) R_{rs} values of the 3×3 vs. 5×5 pixel window.

The water turbidity varies greatly (0–5000 mg/L) [36] as affected by strong tides, coastal currents, and river flow input in Hangzhou Bay. A combined Chl-a retrieval algorithm applicable in both clear and turbid water of Hangzhou Bay is needed. We used a $R_{rs}(745\text{ nm})/R_{rs}(490\text{ nm})$ band ratio to discriminate moderately turbid and extremely turbid water and combined the OC3 algorithm and our improved method.

Using a threshold of 0.4686 for the $R_{rs}(745\text{ nm})/R_{rs}(490\text{ nm})$ band ratio, our GOCI-derived R_{rs} at 159 match-up points were grouped into two categories in moderately turbid water (24) and extremely turbid water (135), as shown in Figure 4. The $R_{rs}(745\text{ nm})/R_{rs}(490\text{ nm})$ band ratio was selected as it has been used in an empirical algorithm (Equations (11) and (12)) for retrieving sediment concentrations ($C_{Sediments}$ ranging from 8 to 5275 mg/L) in Hangzhou Bay by He et al. [36]. Based on the empirical algorithm, a threshold of 0.4686 for $R_{rs}(745\text{ nm})/R_{rs}(490\text{ nm})$ is related to water with $C_{Sediments}$ of 40 mg/L.

$$C_{Sediments} = 10^{1.0758 + 1.1230 \times Ratio} \tag{11}$$

$$Ratio = R_{rs}(745\text{ nm}) / R_{rs}(490\text{ nm}) \tag{12}$$

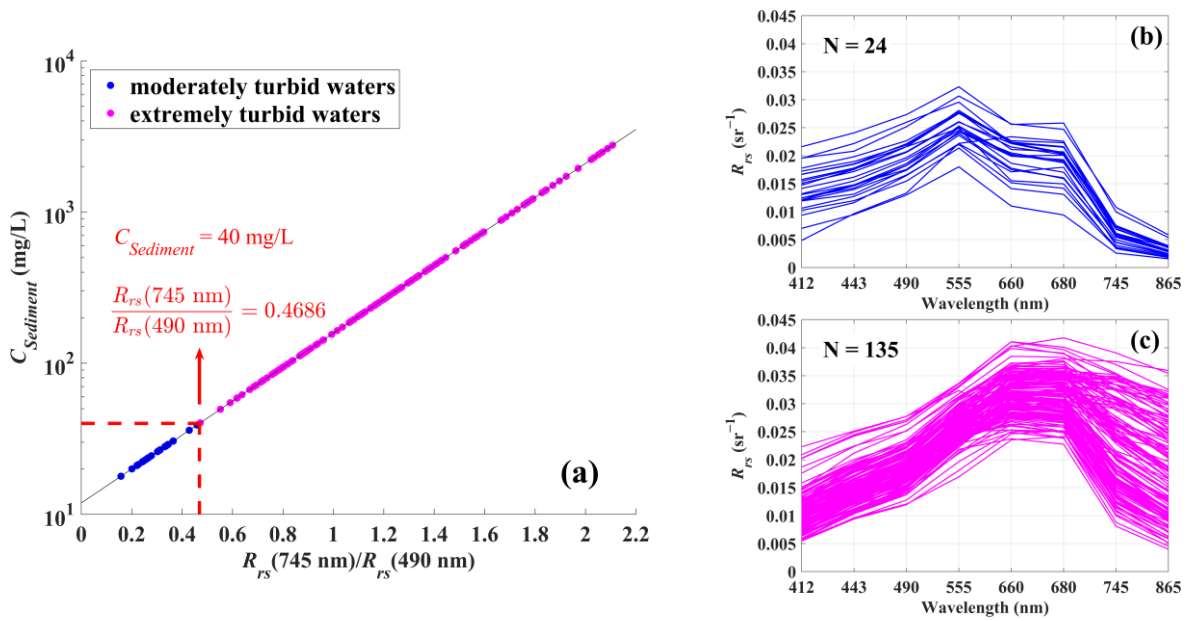


Figure 4. (a) Relationship between the $C_{Sediments}$ and $R_{rs}(745\text{ nm})/R_{rs}(490\text{ nm})$ band ratio. (b) The match-up GOCI-derived R_{rs} spectrum (in blue) in moderately turbid waters ($C_{Sediments}$ from 16.51 to 39.02 mg/L). (c) The match-up GOCI-derived R_{rs} spectrum (in pink) for the extremely turbid waters ($C_{Sediments}$ from 40.05 to 1761.32 mg/L) in Hangzhou Bay.

As seen in Figure 4, the water in Hangzhou Bay is generally turbid, with an obvious “redshift phenomenon”; that is, the reflection peak of the spectrum moves towards the longer red part of the spectrum with increasing water turbidity [37]. A threshold of 0.4686 ($C_{Sediments}$ of 40 mg/L) of the $R_{rs}(745\text{ nm})/R_{rs}(490\text{ nm})$ band ratio can clearly discriminate the water reflectance with moderate or extreme turbidity. The peak spectral value of moderate turbidity water is near the green band (555 nm). The peak value of the spectrum in extremely turbid water moves to longer wavelengths (660–680 nm).

Therefore, we used the OC3 algorithm to invert Chl-a in moderately turbid water and our improved algorithm in extremely turbid water. A threshold of 0.4686 ($C_{Sediments}$ of 40 mg/L) of the $R_{rs}(745\text{ nm})/R_{rs}(490\text{ nm})$ band ratio was used to switch between these two algorithms.

Among the 135 match-ups between field and GOCI data in highly turbid water, 94 were randomly selected as calibration data to develop the Chl-a retrieval algorithm around Hangzhou Bay, and the other 41 were used to validate the algorithm’s performance.

2.6. Accuracy Assessment Indicators

The accuracy of Chl-a concentrations retrieved in this study was evaluated with field measurements using median absolute percentage error (MAPE) and root median square error (RMSE).

$$MAPE = median \left(\left| \frac{C_{retrieved,i} - C_{field,i}}{C_{field,i}} \right| * 100\% \right), i = 1 \dots n \tag{13}$$

$$RMSE = \sqrt{median \left[\left(C_{retrieved,i} - C_{field,i} \right)^2 \right]}, i = 1 \dots n \tag{14}$$

where $C_{retrieved,i}$ and $C_{field,i}$ are the estimated and measured values of Chl-a concentration at sample i , respectively, and n is the total number of samples.

2.7. Spectral Clustering Analysis

In this study, a spectral clustering algorithm was used to analyze the GOCI-derived Chl-a data in 2020 to distinguish the seasonal variation between the Hangzhou Bay and offshore water types. Spectral clustering is a popular clustering algorithm widely used in pattern recognition. It regards data clustering as a graph partitioning problem and makes no assumptions about the form of data clustering [38]. In this study, using GOCI-derived Chl-a data in 2020, median Chl-a values in 4 seasons were first calculated, and a matrix with 4 columns (4 seasons) was derived. The number of rows is equal to the number of valid pixels in each seasonal median data (excluding cloud and land pixels). The 4 columns in the matrices correspond to seasonally median Chl-a concentrations from spring to winter. To avoid errors induced by maximum and minimum values, all data were normalized following Shi and Malik [39]. Then, we carried out cluster analysis using the normalized dataset and the spectral cluster tool in MATLAB. By conducting spectral clustering analysis on curves with different shapes, we selected the optimal cluster number of 4, and these clusters are in accordance with results from Hao et al. [40].

3. Results

3.1. Comparison between R_{rs} Derived in This Study and Operational Level 2 Data Products

The R_{rs} derived in this study was compared with that from concurrent GOCI level 2 products from the KOSC. By comparing 1,494,932 R_{rs} from 5 GOCI datasets (one scene in spring, autumn, and winter and two scenes in summer), the valid R_{rs} of GOCI level 2 products from the KOSC generally agree well with the corresponding data processed in this study (Figure 5). Their average relative percentage differences are 22.57% (412 nm), 15.09% (443 nm), 12.92% (490 nm), 10.22% (555 nm), 21.47% (660 nm), 20.75% (680 nm), 88.24% (745 nm) and 144.91% (865 nm), and their root mean square differences are 0.0025 sr^{-1} (412 nm), 0.0016 sr^{-1} (443 nm), 0.0015 sr^{-1} (490 nm), 0.0014 sr^{-1} (555 nm), 0.0010 sr^{-1} (660 nm), 0.0010 sr^{-1} (680 nm), 0.0010 sr^{-1} (745 nm), and 0.0008 sr^{-1} (865 nm). The rather large percentage differences occur at two near-infrared bands (745 nm, 865 nm) due to the small water reflectance (this can be seen in Figure 6b,d,f,h). In the visible bands, the average relative percentage differences at the blue band (412 nm, 22.57%) are larger than those of the green and red bands (443–680 nm, 10.22–21.47%). Note that the 3 bands of 555, 660, and 680 nm were used in our improved Chl-a retrieval algorithm.

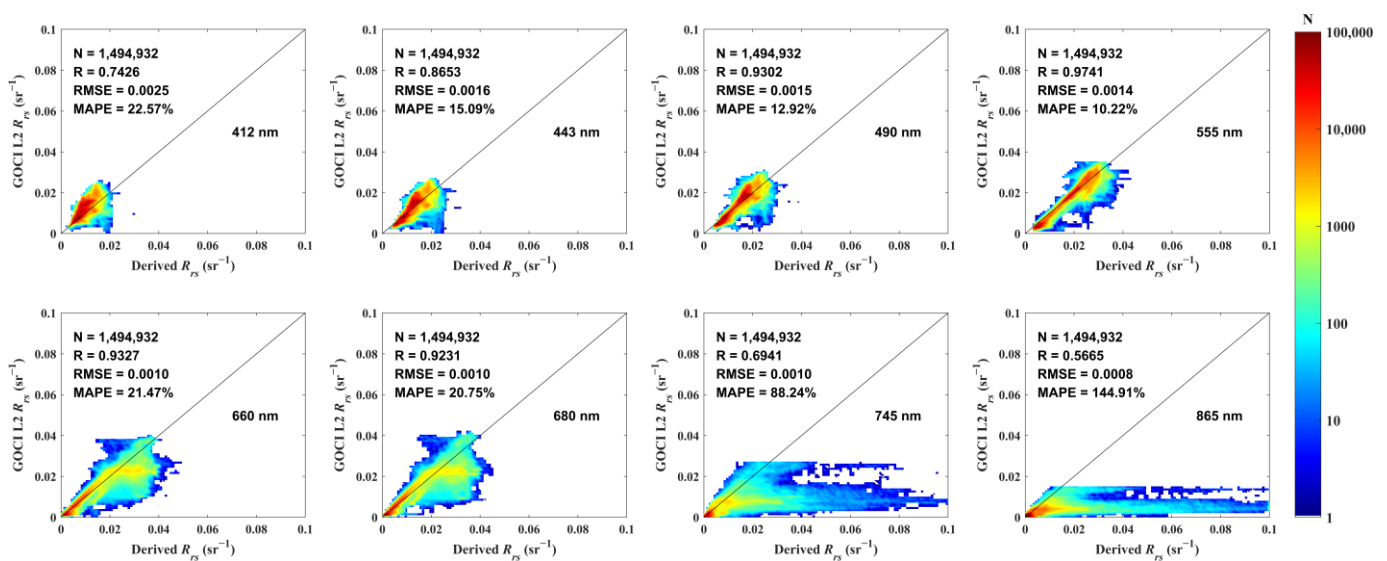


Figure 5. Comparison of valid R_{rs} data pixels from the KOSC's GOCI level 2 products and this study.

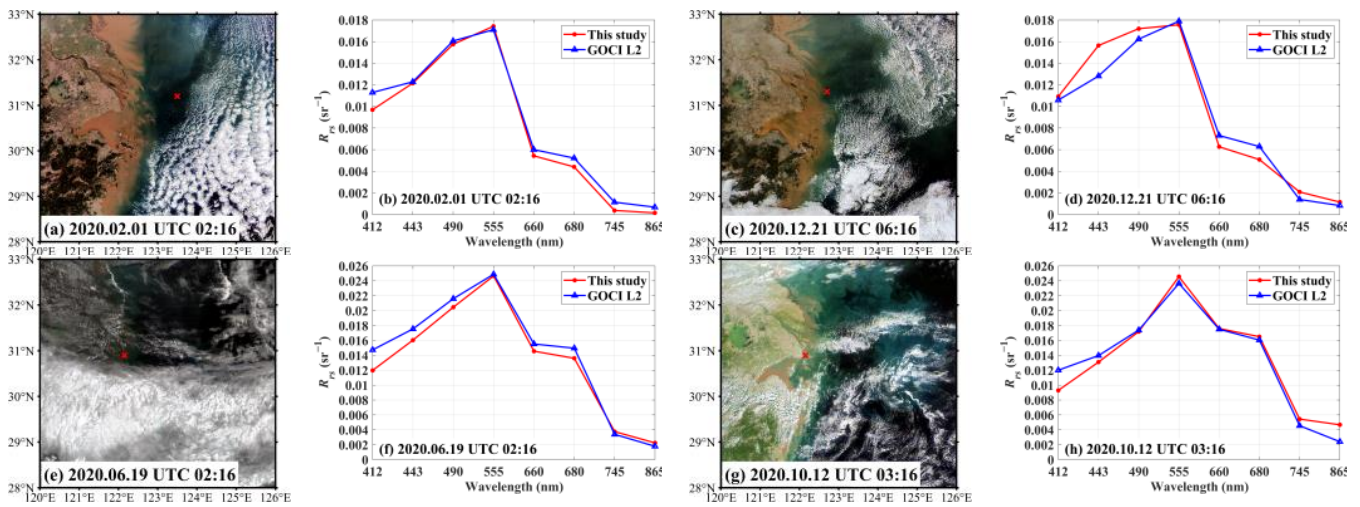


Figure 6. Comparison between GOCI R_{rs} level 2 products (blue triangles) and GOCI R_{rs} from this study (red dots). The results in less turbid water at 02:16 UTC on 1 February 2020 (a,b) and at 06:16 UTC on 21 December 2020 (c,d), in turbid water at 02:16 UTC on 19 June 2020 (e,f) and at 03:16 UTC on 12 October 2020 (g,h). The red crosses (a,c,e,g) indicate locations where R_{rs} spectrums (b,d,f,h) were obtained.

For invalid R_{rs} data pixels in GOCI level 2 products from the KOSC, compared with field data measured in the Yangtze River Estuary and its adjacent coastal sea during the early spring and summer seasons of 2008 by Shen et al. [21], the 135 R_{rs} derived using GOCI data in highly turbid water in this study are similar in spectral shape and amplitude range.

Moreover, this study can derive more valid R_{rs} data in highly turbid water, where the operational level 2 data are usually invalid. In turbid water where Buoys A and B were located during 2020 and 2021, as well as where the cruises were conducted in August 2017 and August 2018, 159 buoy–GOCI match-ups were acquired in this study, while only 24 valid data points were obtained from the KOSC’s GOCI level 2 files. According to the spectrum (Figure 4b), they are all in moderately turbid water. This means that the KOSC’s GOCI level 2 files were valid in the moderately turbid waters and were missing (invalid) in the extremely turbid waters. This indicates that the valid data percentage of GOCI level 2 data from the KOSC in Hangzhou Bay is lower than that in this study.

3.2. The Improved Chl-a Retrieval Algorithm in This Study

Based on the Shen et al. [21] regional algorithm developed for MERIS images in the Yangtze River Estuary and its adjacent water, the R_{rs} at 555, 660, and 680 nm (GOCI bands) were used to replace the 560, 665, and 681 nm (MERIS bands) for λ_1 , λ_3 and λ_4 , and the average of R_{rs} at 555 and 660 nm replaced R_{rs} at 620 nm for λ_2 in Shen et al. [21], as MERIS and GOCI sensors have different bands. Since the GOCI does not have the 620 nm band, we chose the average of 555 and 660 nm as a substitution. Then, we calculated the SCI index values using our GOCI-derived R_{rs} data. The improved regional Chl-a retrieval algorithms were finally obtained by fitting the 94 match-ups of Chl-a data and the SCI values by quadratic polynomial and exponential functions in spring (17), summer (9), autumn (24), and winter (44) (Table 2).

Table 2. Regional Chl-a retrieval algorithms in four seasons in highly turbid water of Hangzhou Bay.

Seasons	Retrieval Algorithms (y :Chl-ain mg/m^3)	N	R	MAPE (%)	RMSE (mg/m^3)
Spring	$y = -113369.64 \times SCI^2 - 866.47 \times SCI - 0.18$	17	0.62	36.76	0.31
Summer	$y = 483762.95 \times SCI^2 - 508.80 \times SCI + 1.28$	9	0.58	33.73	0.58
Autumn	$y = 368596.23 \times SCI^2 - 223.35 \times SCI + 0.94$	24	0.32	72.02	1.00
Winter	$y = 1.596 \times \left(\frac{SCI - 0.0001142}{0.001306} \right)^2$	44	0.38	43.89	0.39

To quantify the accuracy of the retrieval algorithm proposed in this study around Hangzhou Bay, the performance of the improved Chl-a retrieval algorithm in this study was evaluated using calibration and validation data (Figure 7a,b, Table 3). As a reference for comparison, the performance of the OC3 algorithm used in operational GOCI level 2 data products from the KOSC was also demonstrated (Figure 7c, Table 3).

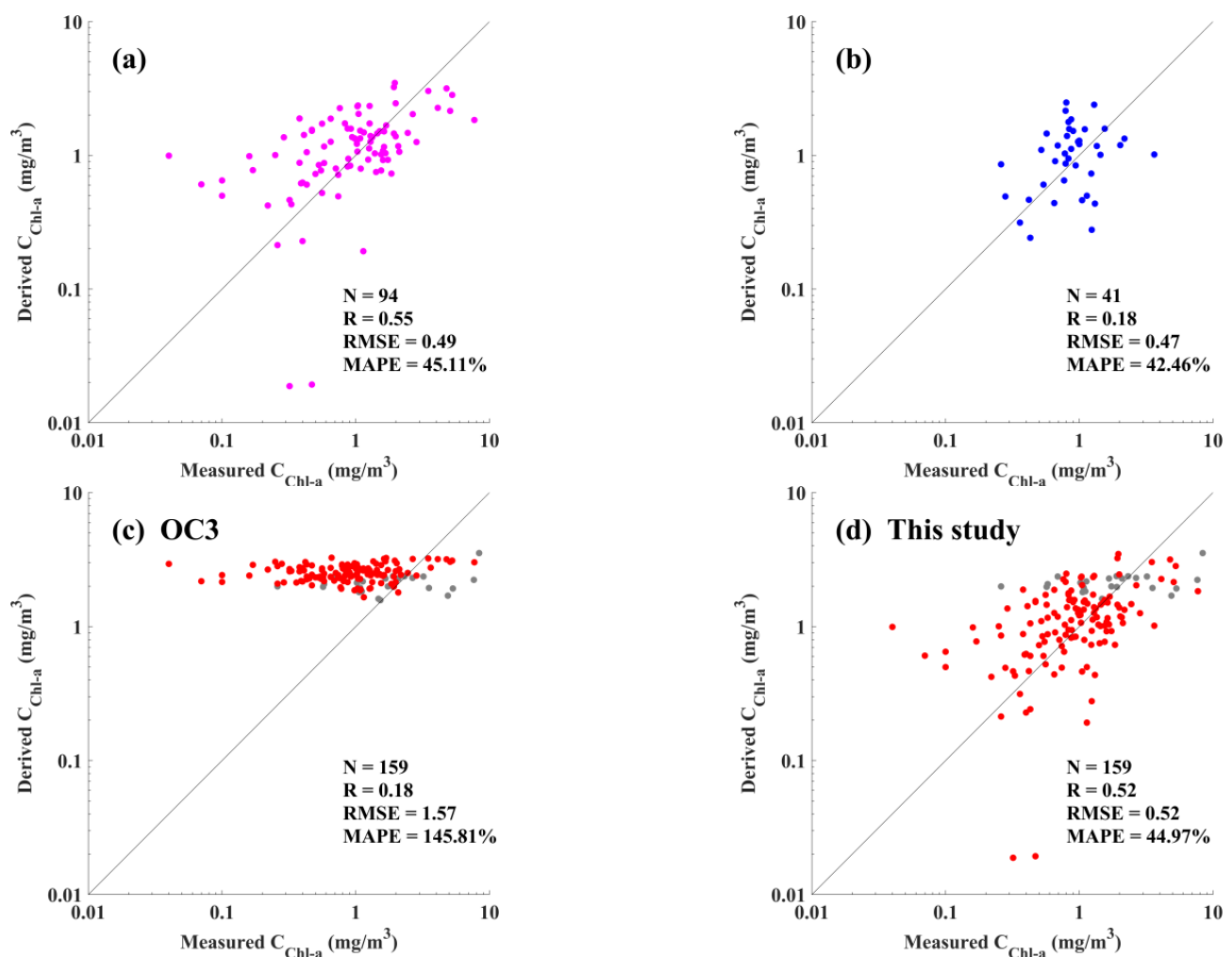


Figure 7. Scatter plot between field Chl-a and the retrieval results from GOCI data. (a) Calibration of 94 match-ups (in pink) in extremely turbid waters, (b) validation of 41 match-ups (in blue) in extremely turbid waters, (c) scatter plots of Chl-a between field data and results derived using OC3, and (d) scatter plots of Chl-a between field data and results derived using the improved method in this study. The retrievals obtained in extremely turbid waters and moderately turbid waters are indicated in red and grey, respectively.

Table 3. Accuracy statistics of the two retrieval algorithms for Chl-a in Hangzhou Bay.

Category	Accuracy Indicator	This Study			OC3		
		All	Extremely Turbid Water	Moderately Turbid Water	All	Extremely Turbid Water	Moderately Turbid Water
Calibration	N	94	94	/	94	94	/
	MAPE (%)	45.11	45.11	/	144.10	144.10	/
	RMSE (mg/m ³)	0.49	0.49	/	1.56	1.56	/
	* P _{±35%} (%)	37.23	37.23	/	13.83	13.83	/
Validation	N	41	41	/	41	41	/
	MAPE (%)	42.46	42.46	/	200.68	200.68	/
	RMSE (mg/m ³)	0.47	0.47	/	1.72	1.72	/
	* P _{±35%} (%)	39.02	39.02	/	4.88	4.88	/
Total	N	159	135	24	159	135	24
	MAPE (%)	44.97	44.85	60.84	145.81	167.05	60.84
	RMSE (mg/m ³)	0.52	0.47	0.86	1.57	1.57	0.86
	* P _{±35%} (%)	37.74	37.78	37.50	15.09	11.11	37.50

* P_{±35%} means proportion of data with uncertainties (absolute percentage error) less than ±35%.

The results from the improved algorithm in this study are generally scattered around the 1:1 line (Figure 7a,b,d), while it appears that there is nearly no relationship between field data and retrievals from OC3, with values mostly around the average of 2.43 mg/m³ (Figure 7c). The MAPE and RMSE of the improved Chl-a algorithm in this study (45.11% and 0.49 mg/m³ for 94 calibration data points, 42.46% and 0.47 mg/m³ for 41 validation data points) are much smaller than those of the OC3 method used in GOCI level 2 data products (144.10% and 1.56 mg/m³ for 94 calibration data points, 200.68% and 1.72 mg/m³ for 41 validation data points). It is worth noting that low correlation coefficients can be observed in Figure 7, and they are supposed to be affected by a few outliers deviating from the 1:1 line, which are mostly in spring and winter.

Using 41 validation data, the MAPE and RMSE of the retrieval results in this study are much smaller in winter (29.12% and 0.25 mg/m³ for 19 data points in winter, not shown in Table 3) than those in other seasons (36.46% and 0.40 mg/m³ for 8 data points in spring, 39.93% and 0.84 mg/m³ for 4 data points in summer, and 79.93% and 0.85 mg/m³ for 10 data points in autumn, not shown in Table 3). Among the four seasons, the accuracy of the retrieval method in this study in autumn is the lowest, though it is better than that of the OC3 algorithm (145.81% and 1.57 mg/m³ for 159 total points).

In extremely turbid water (N = 135), the retrieval results of the OC3 algorithm have more uncertainties (RMSE of 1.72 mg/m³ and MAPE of 200.68% for the validation data; RMSE of 1.57 mg/m³ and MAPE of 167.05% for total data) than this study (RMSE of 0.47 mg/m³ and MAPE of 42.46% for validation data). In moderately turbid water (N = 24), if our improved Chl-a retrieval algorithm for extremely turbid water is applied, the performance of the OC3 algorithm (RMSE of 0.86 mg/m³) seems better than that in this study (RMSE of 0.99 mg/m³, not shown in Table 3). However, both algorithms show large uncertainties in moderately turbid water around Hangzhou Bay.

Considering the uncertainty goal of 35% in SeaWiFS Chl-a concentration in global open ocean waters [41], the percentage of retrievals with MAPE no more than 35% was also calculated. In the extremely turbid water, it accounts for 37.78% for this study and is higher than the 11.11% using OC3. Considering all match-up Chl-a data, it accounts for 37.74% for this study and is 2.5 times higher than the 15.09% for OC3.

3.3. Seasonal Variations in Chl-a in Hangzhou Bay

The seasonal variation in Chl-a in Hangzhou Bay and adjacent coastal water derived by this study (Figure 8b,d,f,h) is more significant than the results of the level 2 data products by the KOSC (Figure 8a,c,e,g). In Figure 8, the Chl-a values in summer and autumn are higher than those in spring and winter for both retrieval methods, while the Chl-a values derived in this study are generally lower than the OC3 values, especially in winter and spring.

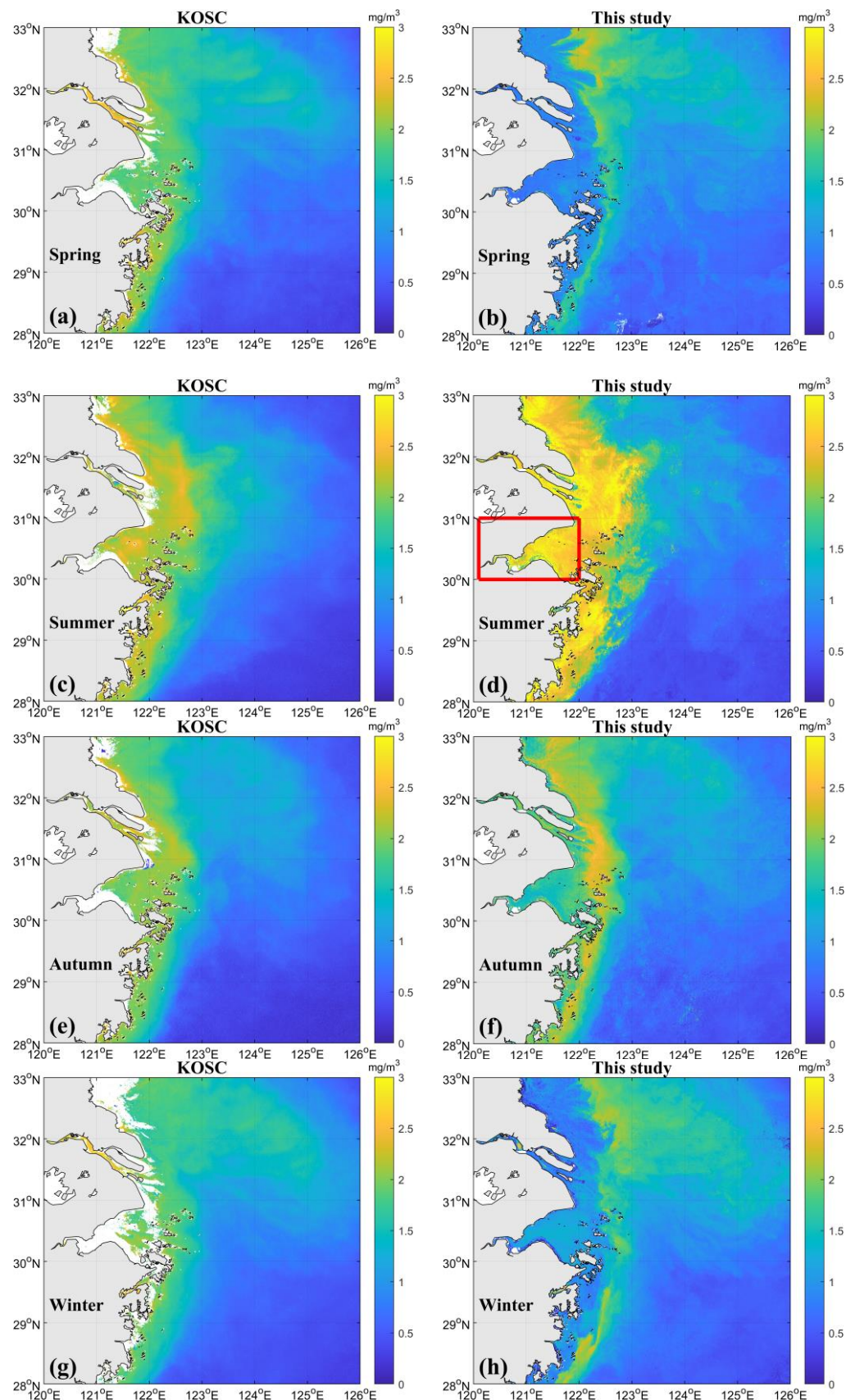


Figure 8. Seasonal averaged maps of Chl-a in Hangzhou Bay and adjacent coastal waters. (a,c,e,g) represent the Chl-a seasonal variation derived by the GOCI level 2 data products of the KOSC, and (b,d,f,h) are the Chl-a seasonal variation derived after atmospheric correction and the improved combined regional Chl-a retrieval algorithm. Hangzhou Bay is indicated in a red rectangle.

To quantitatively demonstrate the seasonal variation, the seasonal mean values of Chl-a collected by the two buoys (A and B) and the GOCI in Hangzhou Bay are listed in Table 4 and Figure 9. A comparison between the Chl-a derived using the GOCI in this study with the KOSC level 2 data product with buoy data shows that the data from the two buoys (0.86–4.38 mg/m³ of Buoy A, 0.98–2.11 mg/m³ of Buoy B) generally vary seasonally, consistent with this study (0.79–2.69 mg/m³ at the location of Buoy A, 0.84–2.65 mg/m³ for Hangzhou Bay), and Chl-a data show the highest values in summer, followed by autumn, and finally spring and winter. However, the GOCI Chl-a values (1.80–2.15 mg/m³ at the location of Buoy A, 1.93–2.27 mg/m³ for Hangzhou Bay) from OC3 do not vary much throughout the year, although the Chl-a average in summer is slightly higher than that in other seasons.

Table 4. Comparison of seasonal mean Chl-a values from buoys and GOCI data in Hangzhou Bay (HZB) (mg/m³).

	Spring	Summer	Autumn	Winter
Chl-a of Buoy A	1.07 ± 0.67	4.38 ± 3.25	1.57 ± 1.57	0.86 ± 0.57
Chl-a of Buoy A (excluding extremely high Chl-a values in summer) *	1.07 ± 0.67	3.35 ± 2.85	1.57 ± 1.57	0.86 ± 0.57
Chl-a of Buoy B	0.98 ± 0.56	2.11 ± 2.71	1.17 ± 1.02	1.10 ± 0.67
GOCI Chl-a of this study at Buoy A	0.79 ± 0.48	2.69 ± 2.31	1.90 ± 0.64	1.04 ± 0.45
GOCI Chl-a of the KOSC at Buoy A	1.80 ± 0.16	2.15 ± 0.25	2.03 ± 0.25	1.87 ± 0.20
GOCI Chl-a of this study in HZB	0.84 ± 0.17	2.65 ± 0.33	1.61 ± 0.28	1.12 ± 0.29
GOCI Chl-a of the KOSC in HZB	1.93 ± 0.30	2.27 ± 0.29	2.00 ± 0.34	1.99 ± 0.29

* Chl-a of Buoy A (excluding extremely high Chl-a values in summer) means that the long-term high Chl-a concentrations at Buoy A in summer in 2020 have not been taken into account (high Chl-a values ranging from 20 to 98.62 mg/m³ from 13 June to 15 June, 20 July to 29 July, 2 August to 3 August, and 10 August to 19 August).

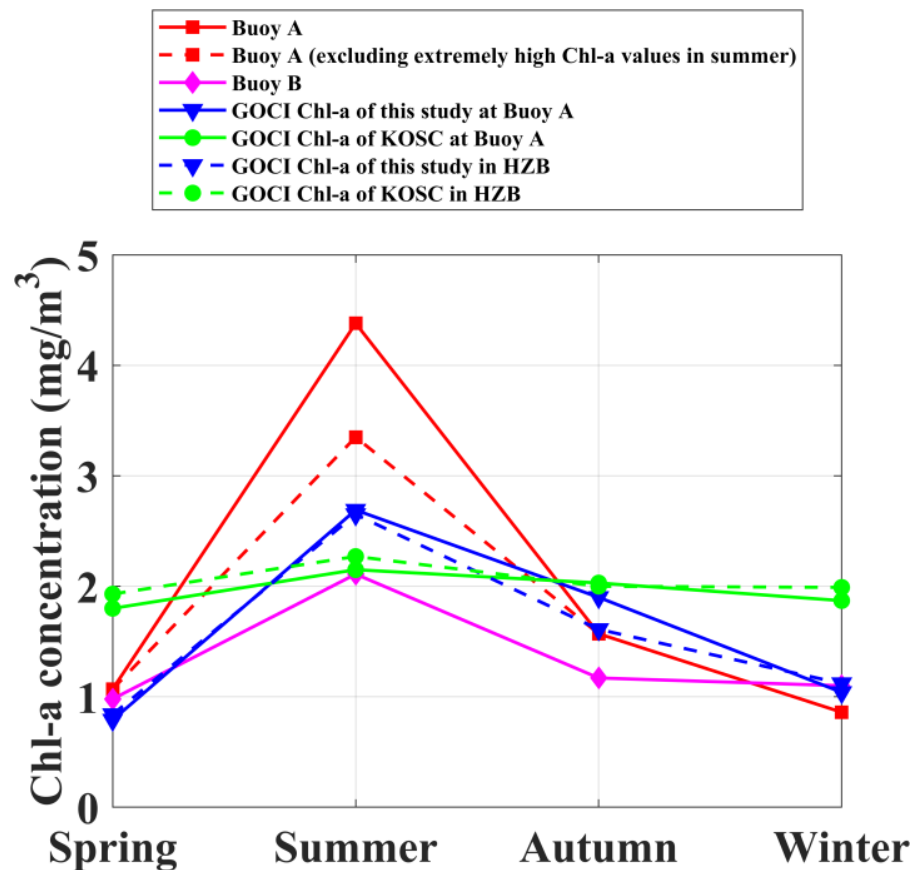


Figure 9. Seasonal mean values of Chl-a from buoys and GOCI data in Hangzhou Bay (HZB).

Note that the Chl-a values of Buoy A in 2020 have a much higher average in the summer than Buoy B in 2021. High Chl-a concentrations occurred frequently at Buoy A in summer in 2020. Specifically, the time series data of Buoy A have extremely high Chl-a values ranging from 20 to 98.62 mg/m³ from 13 June to 15 June, 20 July to 29 July, 2 August to 3 August, and 10 August to 19 August. We checked that these high Chl-a signals cannot be inferred from spectral characteristics of the GOCI R_{rs} data. Then the seasonal average values including and excluding the portion of extremely high Chl-a data at Buoy A in summer were calculated (4.38 mg/m³ versus 3.35 mg/m³), respectively, and results are presented in Figure 9 and Table 4. Compared with the GOCI level 2 data product from the KOSC at Buoy A in summer (2.15 ± 0.25 mg/m³), the seasonal average derived using GOCI data at Buoy A in this study (2.69 ± 2.31 mg/m³) is closer to that calculated using Buoy A measurements by excluding the portion of extremely high Chl-a data.

In Figure 8, the Chl-a concentrations showed a zonal distribution along the longitude from coastal Hangzhou Bay to offshore water. The concentrations of Chl-a generally show a low, high, and low trend from coastal to offshore water in spring, autumn, and winter, respectively. The KOSC level 2 data generally show high values in coastal waters and low values in offshore waters.

To compare this Chl-a zonal variation from nearshore to offshore, we selected a transect indicated by A to E in the study area (Figure 10). The Chl-a from the KOSC generally agrees well with this study in coastal and offshore water (from B to E) and has higher values than this study in Hangzhou Bay in spring, autumn, and winter. The retrieved Chl-a in this study shows a zonal distribution trend of low, high, and low from Hangzhou Bay to offshore water in winter, autumn, and spring, while Chl-a data from the KOSC have no such trend. Both the Chl-a retrieved in this study and the Chl-a data from the KOSC show high values in coastal waters and low values in offshore waters in summer. In addition, these trends in this study are similar to the results from Zhang et al. [42] based on their field measurements in 2008.

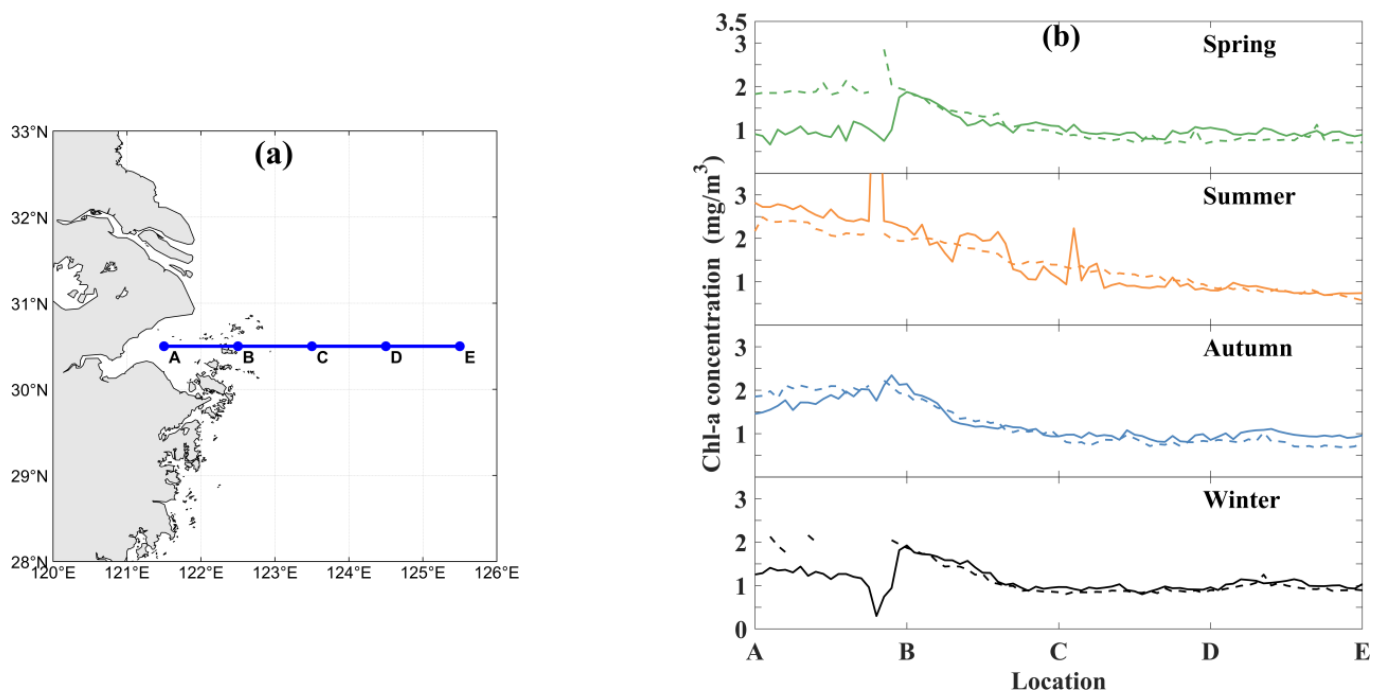


Figure 10. The Chl-a seasonal variation in the study area retrieved by the GOCI. (a) The location of the selected representative transect indicated by A to E in the study area. (b) The seasonal variations in Chl-a at the representative transect (the dashed line represents the GOCI Chl-a of the KOSC, and the solid line is the Chl-a of this study).

3.4. Classification of Chl-a Seasonal Cycle

As shown in Figure 11, the four seasonal cycles in Chl-a in 2020 correspond to four areas from coastal to offshore water: (1) Hangzhou Bay and its adjacent areas (P area) with significant seasonal cycles, where high values of Chl-a occur in summer and low values occur in spring and winter; (2) nearshore area (Q area) with distinct seasonal variations, where high values of Chl-a occur in summer and the lowest values occur in autumn, and the average Chl-a is about 1.5 mg/m³; (3) offshore area (M area) with seasonal variations, where the highest Chl-a occurs in winter and the lowest in summer, and the average Chl-a is lower than 1 mg/m³; and (4) open sea (N area), where Chl-a is low (approximately 0.5 mg/m³) and the seasonal variation is not significant. With the increase in offshore distance, both the Chl-a concentration levels and seasonal variations for the four areas exhibit a decreasing trend. The most significant seasonal variation of Hangzhou Bay and its adjacent areas (P area) can be seen in this study, while it cannot be observed from the GOCI operational L2 data in 2020 (Figures 8 and 9).

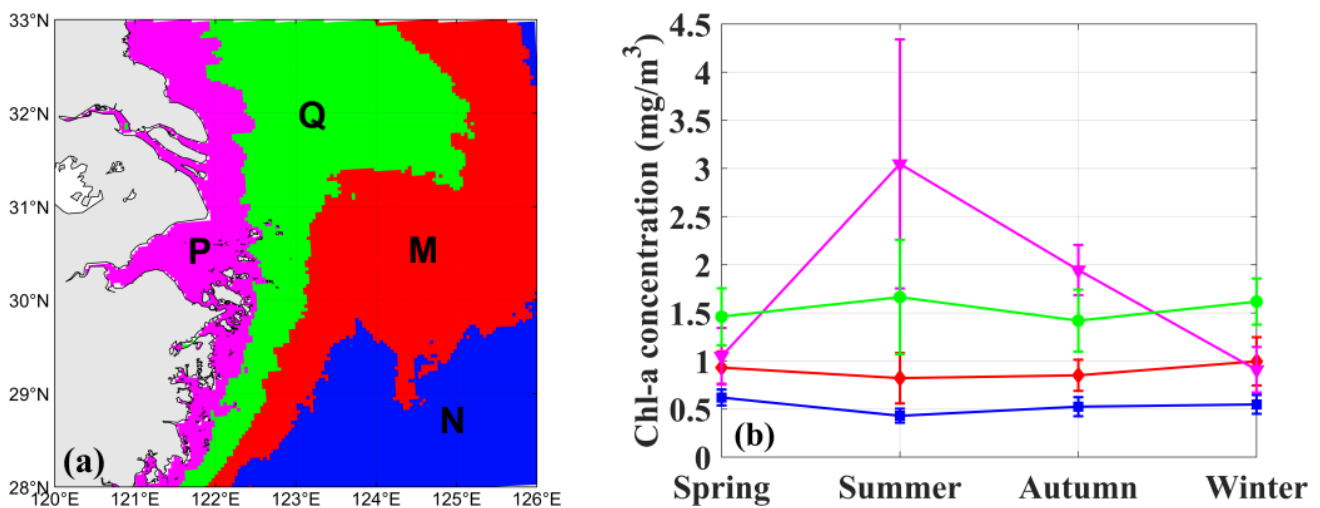


Figure 11. Different Chl-a seasonal cycle types in 2020 in the study area: (a) distribution of four Chl-a seasonal cycle types: Hangzhou Bay and its adjacent areas (P area, in pink), nearshore area (Q area, in green), offshore area (M area, in red), and open sea (N area, in blue); (b) seasonal Chl-a variations for different types (the pink, green, red and blue lines represent the P, Q, M and N areas, respectively).

4. Discussion

4.1. Comparison of Multitemporal Observations for Hangzhou Bay

Different spaceborne water color sensors observe the ocean at different times. It is well known that sensors with high temporal and spatial resolutions have great advantages in monitoring dynamic systems. We quantified the accuracy and difference of single, dual, or multitemporal observations (polar-orbiting or geostationary orbiting ocean color sensors) using continuously measured buoy data in Hangzhou Bay. The accuracy and difference are calculated using buoy data and not using satellite data. This can exclude the difference from calibrations and corrections of different satellite sensors.

The polar-orbiting sensors of MODIS-Aqua and MODIS-Terra and the geostationary sensors of the GOCI are commonly used in various studies. MODIS-Aqua and MODIS-Terra usually take measurements at approximately 02:30 or 05:30 UTC, and GOCI acquired images 8 times per day in hourly intervals from 00:15 to 07:45 UTC. Before choosing suitable data from different data products in studies, it is necessary to know how the accuracy and difference of observations at different temporal frequencies vary.

To quantify the difference in Chl-a observations in the 24 h temporal (buoy), multi-temporal (buoy data at GOCI time), dual-temporal (buoy data at MODIS-A and MODIS-T time), and single-temporal (buoy data at MODIS-T time) ranges in Hangzhou Bay, the Buoy

All data were averaged at 24 h (daily average), 8 h (at GOCI time), 2 h (at MODIS-Aqua and MODIS-Terra time), and 1 h (at MODIS-Terra time) and compared (Figure 12).

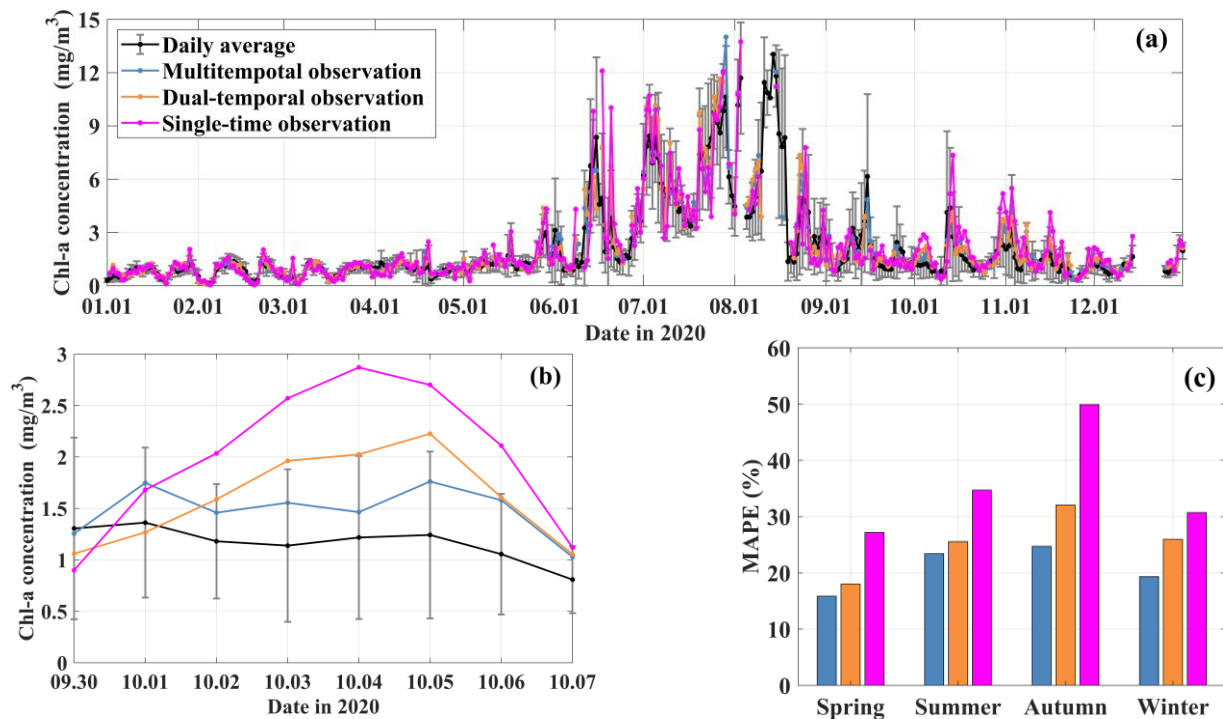


Figure 12. Chl-a comparison among the 8 h multitemporal (in blue), dual-temporal (in yellow), and single-time (in pink) observations and the 24 h daily (in black) averages. (a) Comparison of the time series in 2020. (b) Comparison of the time series from 30 September to 7 October 2020. (c) The mean average percentage errors of three temporal observations (8 h multitemporal in blue, dual-temporal in yellow, single-time in pink) in four seasons compared with the 24 h daily averages.

As shown in Figure 12a, different temporal-range averages can generally follow the 24 h daily averages well throughout 2020. However, as shown in Figure 12b, the daily averages of the 8 h multitemporal observations are the closest to the results of the 24 h daily averages, in both the trend and value. The trend and value of the single-time observation show the largest difference from the 24 h daily average. The trend of dual-temporal observations is consistent with that of single-time observations. As shown in Figure 12c, the mean absolute percentage error of the multitemporal observation is the lowest (approximately 15–25%), then the dual-temporal observation (approximately 15–35%), and finally the single observation (approximately 25–50%). The three observation methods have the largest MAPE in autumn and the smallest MAPE in spring. This shows that multitemporal observations are more accurate, and the GOCI has advantages in monitoring dynamic coastal areas than other low-temporal polar-orbiting sensors. However, when multitemporal observations are not available for analyzing seasonal variations, the dual-temporal average can be a good substitute. For a short-term change study of daily averaged Chl-a, multitemporal observations are needed in Hangzhou Bay. Note that this analysis is based on data from Buoy A in Hangzhou Bay in 2020. The accuracy and difference should differ spatially and could vary temporally.

4.2. Seasonal Variation in Chl-a in Hangzhou Bay

Previous studies have studied the Chl-a seasonal cycle using field data [42–44] or spaceborne ocean color data [45,46] in the East China Seas. However, Chl-a retrievals are not accurate in coastal turbid water [47]. Typically, Chl-a data are missing in operational ocean color products in the highly turbid coastal water of Hangzhou Bay and its adjacent coastal water (Figure 8). The Chl-a seasonal cycles in Hangzhou Bay and its adjacent coastal

waters have not been fully described in previous studies. Therefore, we demonstrated a typical Chl-a seasonal cycle in Hangzhou Bay and its adjacent coastal water in 2020. This could vary with time, and needs to be further validated using more field and satellite data. However, this would be helpful for studies on different factors affecting varying Chl-a seasonal cycles in Hangzhou Bay and adjacent coastal waters.

In spring and winter, the concentration of Chl-a in Hangzhou Bay and the Yangtze River Estuary is lower than that in the open sea area, while in summer and autumn, it is much higher than that in the open sea area, which is related to the water temperature and input and diffusion of nutrients from the land [48].

In summer, southerly winds prevail in the study area, and the surface water temperature is the highest year-round. The runoff of the Yangtze River is in the rainy season, and a large amount of fresh water is injected and diffused, carrying a large amount of sediment and nutrients [43]. The concentration of Chl-a in Hangzhou Bay and the Yangtze River Estuary is higher than that in the open seas. The high value area of Chl-a nearshore weakened in autumn, which may be due to less sunshine and lower water temperature than that in summer.

In winter, northerly winds prevail in the study area, the temperature drops sharply, and the surface water temperature drops. At this time, the runoff of the Yangtze River is in the dry season, and the diluted water of the Yangtze River is weak [43]. The content of Chl-a in Hangzhou Bay decreased significantly and presented a zonelike distribution in space, with the highest value at approximately 123° E and decreasing to the east and west, which was consistent with the research results of Zhang et al. [49]. In spring, with increasing water temperature, the concentration of Chl-a in Hangzhou Bay and the Yangtze River Estuary increases slowly.

4.3. Limitations of the Atmospheric Correction Procedure and Retrieval Algorithms in This Study

In the atmospheric correction procedure of this study, the cloud masking method is from Lu et al. [34], which is designed for the GOCI and used in Chinese coastal turbid water. Although this method is supposed to be applied to almost all other ocean color sensors, the threshold values are supposed to be slightly adjusted depending on the specific sensor, such as MODIS. Its performance also varies from water to water; for example, it could retain some thin cloudy pixels in less turbid water [34]. In terms of the aerosol contribution correction procedure based on Hu et al. [9] in this study, for other specific research areas and ocean color sensors, the range of L_a in less turbid water should be modified accordingly. Thus, the constant parameters in our atmospheric correction procedure are region- and sensor-specific and need to be adjusted according to different local regions and sensors. It should be noted that the R_{rs} derived in extremely turbid water in this study were not validated using synchronous field data, and thus, the performance of the atmospheric correction procedure of this study needs to be further verified in the future.

Differences in R_{rs} derived in this study and the KOSC's GOCI L2 data can be observed in less turbid water (Figures 5 and 6). Therefore, there is also a slight difference in Chl-a concentrations (RMSE of 0.16 mg/m³, not shown) in offshore water (Figure 8). However, our seasonal trends are similar to the results from Hao et al. [40]. Considering that our study is mainly concentrated in Hangzhou Bay and the adjacent coastal water, these differences in the offshore sea are not assessed in this study. Further research on merging coastal results with offshore data products is needed.

Using the 159 match-up Chl-a data in the range of 0.01 to 10 mg/m³, the retrieval method of Chl-a in this study is developed with better accuracy (MAPE of 44.97%, RMSE of 0.52 mg/m³) than OC3. Note that the high Chl-a data of Buoy A in summer were not used. We checked that these high Chl-a signals cannot be inferred from spectral characteristics of the GOCI R_{rs} data. We speculated that the high Chl-a events of Buoy A in 2020 could occur in a very small spatial area. Alternatively, high Chl-a might cause high reflectance in the near-infrared when forming surface algae blooms; however, in the sediment-laden water, the high near-infrared reflectance resulted from both the high Chl-a [50] and the

high sediment concentrations [51], which are difficult to be distinguished. Using limited match-ups in summer, a larger RMSE of the Chl-a algorithm (0.84 mg/m^3 for 4 validation match-ups) can be observed. In addition, the larger MAPE and RMSE can also be observed in autumn (72.02% and 1.00 mg/m^3 for 24 calibration data, 79.93% and 0.85 mg/m^3 for 10 validation data) in Section 3.2. Thus, the performance of our approach in summer and autumn needs to be further validated or improved using more field data. As noted in Section 3.2, low correlation coefficients are observed in Figure 7, and they are supposed to be affected by a few match-up outliers in spring and winter. In spring and winter, the water in Hangzhou Bay is extremely turbid, and the Chl-a concentrations are low (Figure 8). We speculate that the outliers could be due to the noises in field measurements of buoy Chl-a, or due to the error in spectral R_{rs} from the atmospheric correction procedure in turbid water. The correlation coefficients between field Chl-a and GOCI-derived R_{rs} could be further improved when more match-up data samples can be obtained in the future. Additionally, since the GOCI does not have the 620 nm band as MERIS, in this study, we chose the average of R_{rs} at 555 and 660 nm as a substitution for R_{rs} at 620 nm using the SCI in Shen et al. [21]. This could increase the Chl-a estimation uncertainties using the GOCI (from June 2010 to March 2021, 500 m spatial resolution), and the retrieval accuracy could be further improved when the GOCI-II data (with a 620 nm band, launched in February 2020, 250 m spatial resolution) are continuously to be used in the future. Moreover, in moderately turbid water, using our limited match-up data ($N = 24$), although the performance of the OC3 algorithm (RMSE of 0.86 mg/m^3) seems better than that in this study (RMSE of 0.99 mg/m^3 , not shown in Table 3, mentioned in Section 3.2), the performance of OC3 needs to be further improved using more field data.

Synoptic seasonal maps of Chl-a in Hangzhou Bay in 2020 were derived using GOCI data in this study. Many data are missing for seasonally averaged Chl-a data products from the KOSC due to the highly turbid water and frequent clouds in Hangzhou Bay and coastal water (Figure 8a,c,e,g); however, the synoptic seasonal maps of Chl-a derived by this study have more valid data in Hangzhou Bay, as more data can be retrieved over cloudless highly turbid water (Figure 8b,d,f,h). This proves the better performance of this study in obtaining more valid data over highly turbid water. Of particular note is that the Chl-a values in this study seem to have much noise in summer (Figure 10b), which may be because the cloud masking method is designed for turbid waters, which could misjudge some thin cloud pixels as water. However, compared with published studies using field data [42–44] or spaceborne ocean color data [40,46] in East China Seas, our GOCI-derived Chl-a data in 2020 generally show consistent seasonal and spatial variations. For example, based on field measurements, Shen et al. [43] found that there was a clear peak area of Chl-a concentration near the Yangtze River Estuary in summer in 1988 and 1989, Wang et al. [44] noted that the high Chl-a concentration in Hangzhou Bay appeared in summer in 2006, and Zhang et al. [42] demonstrated that the Chl-a concentration in the coastal area had a significant seasonal variation in 2008. Based on the spaceborne ocean color data, Sha et al. [46] pointed out that the annual variation range of Chl-a concentration in distant seawaters is small using MODIS data from 2002 to 2007; Hao et al. [40] indicated that summer bloom occurred frequently in coastal seas around East China Seas using the OC-CCI dataset from 1998 to 2013, and the OC-CCI dataset is merged from MODIS, SeaWiFS, and MERIS data. Although our results seem reasonable compared with our two buoys, as well as previous studies, the accuracy should be further checked using more data in Hangzhou Bay over a longer temporal range.

5. Conclusions

The geostationary ocean color sensor GOCI offers good opportunities to study diurnal variabilities in coastal environment dynamics. However, in the typical sediment-laden turbid water in Hangzhou Bay, valid ocean color parameters in operational data products are missing. In this study, the Chl-a concentrations in Hangzhou Bay were derived with GOCI data in August 2017 and August 2018 and from 2020 to 2021 by using an existing

atmospheric correction procedure and an improved Chl-a retrieval method in Hangzhou Bay. Compared with the OC3 method used in the GOCI level 2 data product of the KOSC, this study improves the valid Chl-a data sample number (from 24 to 159), and the proportion of Chl-a data within an uncertainty of less than $\pm 35\%$ increased by 2.5 times. The seasonal variation in Chl-a in Hangzhou Bay and adjacent coastal waters in 2020 was also presented. The Chl-a retrievals of this study are more consistent with buoy data than the GOCI level 2 data products from the KOSC in Hangzhou Bay. This study offers a scheme to obtain comparatively accurate Chl-a retrievals using the GOCI in the highly turbid water of Hangzhou Bay and effectively increases the reliability of chlorophyll inversions using the GOCI. This could offer insight into the spatial and seasonal variations in Chl-a in Hangzhou Bay using the GOCI.

Author Contributions: Conceptualization, S.H.; data collection, C.Z. and X.M.; methodology, Y.Y. and L.W.; writing—original draft preparation, Y.Y.; writing—review and editing, S.H., Y.Y. and Y.G.; supervision, S.H., Y.G. and P.L.; funding acquisition, S.H. and P.L. All authors have read and agreed to the published version of the manuscript.

Funding: This research was funded by the Hainan Provincial Natural Science Foundation of China, grant number 420QN289; the Scientific and Technological Project of Zhoushan, grant number 2022C81010; the National Natural Science Foundation of China, grant number 41876031; and the High-Level Personnel of Special Support Program of Zhejiang Province, grant number 2019R52045.

Institutional Review Board Statement: Not applicable.

Informed Consent Statement: Not applicable.

Data Availability Statement: Not applicable.

Acknowledgments: We thank the Shanghai Marine Monitoring and Forecasting Center for providing the buoy data. We thank the Observation and Research Station of Marine Ecosystem in the Yangtze River Estuary, Ministry of Natural Resources, for providing cruise data. We thank the Korea Ocean Satellite Center for providing the GOCI data and the GDPS software. We thank the National Aeronautics and Space Administration for the SeaDAS software. We thank the Hainan Provincial Observatory of Ecological Environment and Fishery Resource in Yezhou Bay, for help with instrument calibration.

Conflicts of Interest: The authors declare no conflict of interest.

References

1. Miranda, J.; Baliarsingh, S.K.; Lotliker, A.A.; Sahoo, S.; Sahu, K.C.; Kumar, T.S. Long-term trend and environmental determinants of phytoplankton biomass in coastal waters of northwestern Bay of Bengal. *Environ. Monit. Assess.* **2020**, *192*, 55. [[CrossRef](#)] [[PubMed](#)]
2. Cullen, J. The deep chlorophyll maximum—Comparing vertical profiles of chlorophyll-a. *Can. J. Fish. Aquat. Sci.* **1982**, *39*, 791–803. [[CrossRef](#)]
3. Steele, J. Environmental control of photosynthesis in the Sea. *Limnol. Oceanogr.* **1962**, *7*, 137–150. [[CrossRef](#)]
4. Costa, D.D.S.; Jansen Cutrim, M.V. Spatial and seasonal variation in physicochemical characteristics and phytoplankton in an estuary of a tropical delta system. *Reg. Stud. Mar. Sci.* **2021**, *44*, 101746. [[CrossRef](#)]
5. Tian, B.; Wu, W.; Yang, Z.; Zhou, Y. Drivers, trends, and potential impacts of long-term coastal reclamation in China from 1985 to 2010. *Estuar. Coast. Shelf. Sci.* **2016**, *170*, 83–90. [[CrossRef](#)]
6. Dasgupta, S.; Singh, R.P.; Kafatos, M. Comparison of global chlorophyll concentrations using MODIS data. *Adv. Space Res.* **2009**, *43*, 1090–1100. [[CrossRef](#)]
7. Antoine, D. *Ocean-Colour Observations from a Geostationary Orbit*; International Ocean Color Coordinating Group (IOCCG): Dartmouth, NS, Canada, 2012. Available online: <https://repository.oceanbestpractices.org/handle/11329/523> (accessed on 4 December 2022).
8. Ryu, J.; Han, H.; Cho, S.; Park, Y.; Ahn, Y. Overview of Geostationary Ocean Color Imager (GOCI) and GOCI Data Processing System (GDPS). *Ocean Sci. J.* **2012**, *47*, 223–233. [[CrossRef](#)]
9. Hu, C.; Carder, K.L.; Muller-Karger, F.E. Atmospheric correction of SeaWiFS imagery over turbid coastal waters: A practical method. *Remote Sens. Environ.* **2000**, *74*, 195–206. [[CrossRef](#)]
10. Wang, M.; Shi, W. Estimation of ocean contribution at the MODIS near-infrared wavelengths along the east coast of the U.S.: Two case studies. *Geophys. Res. Lett.* **2005**, *32*, L13606. [[CrossRef](#)]
11. Wang, M.; Shi, W.; Tang, J. Water property monitoring and assessment for China's inland Lake Taihu from MODIS-Aqua measurements. *Remote Sens. Environ.* **2011**, *115*, 841–854. [[CrossRef](#)]

12. Bai, R.; He, X.; Bai, Y.; Gong, F.; Zhu, Q.; Wang, D.; Li, T. Atmospheric correction algorithm based on the interpolation of ultraviolet and shortwave infrared bands. *Opt. Express* **2023**, *31*, 6805–6826. [[CrossRef](#)] [[PubMed](#)]
13. Tian, L.; Zeng, Q.; Tian, X.; Li, J.; Wang, Z.; Li, W. Water environment remote sensing atmospheric correction of Geostationary Ocean Color Imager data over turbid coastal waters in the Bohai Sea using artificial neural networks. *Curr. Sci.* **2016**, *110*, 1079–1085. [[CrossRef](#)]
14. Wang, J.; Wang, Y.; Lee, Z.; Wang, D.; Chen, S.; Lai, W. A revision of NASA SeaWiFS atmospheric correction algorithm over turbid waters with artificial Neural Networks estimated remote-sensing reflectance in the near-infrared. *Isprs. J. Photogramm.* **2022**, *194*, 235–249. [[CrossRef](#)]
15. Gordon, H.; Wang, M. Retrieval of water-leaving radiance and aerosol optical-thickness over the oceans with SeaWiFS—A preliminary algorithm. *Appl. Opt.* **1994**, *33*, 443–452. [[CrossRef](#)]
16. Howard, R.; Gordon, A.Y.M. *Remote Assessment of Ocean Color for Interpretation of Satellite Visible Imagery*; Springer: London, UK, 1983; ISBN 9780387909233.
17. O'Reilly, J.E.; Werdell, P.J. Chlorophyll algorithms for ocean color sensors—OC4, OC5 & OC6. *Remote Sens. Environ.* **2019**, *229*, 32–47. [[CrossRef](#)]
18. O'Reilly, J.E.; Maritorena, S.; Mitchell, B.G.; Siegel, D.A.; Carder, K.L.; Garver, S.A.; Kahru, M.; McClain, C. Ocean color chlorophyll algorithms for SeaWiFS. *J. Geophys. Res.* **1998**, *103*, 24937–24953. [[CrossRef](#)]
19. Kim, W.; Moon, J.; Park, Y.; Ishizaka, J. Evaluation of chlorophyll retrievals from Geostationary Ocean Color Imager (GOCI) for the North-East Asian region. *Remote Sens. Environ.* **2016**, *184*, 482–495. [[CrossRef](#)]
20. Gilerson, A.A.; Gitelson, A.A.; Zhou, J.; Gurlin, D.; Moses, W.; Ioannou, I.; Ahmed, S.A. Algorithms for remote estimation of chlorophyll-a in coastal and inland waters using red and near infrared bands. *Opt. Express* **2010**, *18*, 24109–24125. [[CrossRef](#)]
21. Shen, F.; Zhou, Y.; Li, D.; Zhu, W.; Salama, M.S. Medium resolution imaging spectrometer (MERIS) estimation of chlorophyll-a concentration in the turbid sediment-laden waters of the Changjiang (Yangtze) Estuary. *Int. J. Remote Sens.* **2010**, *31*, 4635–4650. [[CrossRef](#)]
22. Zhang, F.; Zhang, B.; Li, J.; Shen, Q.; Wu, Y.; Wang, G.; Zou, L.; Wang, S. Validation of a synthetic chlorophyll index for remote estimates of chlorophyll-a in a turbid hypereutrophic lake. *Int. J. Remote Sens.* **2014**, *35*, 289–305. [[CrossRef](#)]
23. Siswanto, E.; Tang, J.; Yamaguchi, H.; Ahn, Y.; Ishizaka, J.; Yoo, S.; Kim, S.; Kiyomoto, Y.; Yamada, K.; Chiang, C.; et al. Empirical ocean-color algorithms to retrieve chlorophyll-a, total suspended matter, and colored dissolved organic matter absorption coefficient in the Yellow and East China Seas. *J. Oceanogr.* **2011**, *67*, 627–650. [[CrossRef](#)]
24. Lins, R.C.; Martinez, J.; Marques, D.D.M.; Cirilo, J.A.; Fragoso, C.R. Assessment of chlorophyll-a remote sensing algorithms in a productive tropical estuarine-lagoon system. *Remote Sens.* **2017**, *9*, 516. [[CrossRef](#)]
25. Le, C.; Li, Y.; Zha, Y.; Sun, D.; Huang, C.; Lu, H. A four-band semi-analytical model for estimating chlorophyll a in highly turbid lakes: The case of Taihu Lake, China. *Remote Sens. Environ.* **2009**, *113*, 1175–1182. [[CrossRef](#)]
26. Yi, C.; An, J. A four-band quasi-analytical algorithm with MODIS bands for estimating chlorophyll-a concentration in turbid coastal waters. *J. Indian Soc. Remote* **2014**, *42*, 839–850. [[CrossRef](#)]
27. Lee, Z.; Carder, K.L. Absorption spectrum of phytoplankton pigments derived from hyperspectral remote-sensing reflectance. *Remote Sens. Environ.* **2004**, *89*, 361–368. [[CrossRef](#)]
28. Hu, Y.; Yu, Z.; Zhou, B.; Li, Y.; Yin, S.; He, X.; Peng, X.; Shum, C.K. Tidal-driven variation of suspended sediment in Hangzhou Bay based on GOCI data. *Int. J. Appl. Earth Obs.* **2019**, *82*, 101920. [[CrossRef](#)]
29. Shi, J.Z. Tide-induced fine sediment resuspension in the well-mixed Hangzhou Bay, East China Sea, China. *Earth Environ. Sci. Trans. R. Soc. Edinb.* **2011**, *102*, 25–34. [[CrossRef](#)]
30. Feng, J.; Chen, H.; Zhang, H.; Li, Z.; Yu, Y.; Zhang, Y.; Bilal, M.; Qiu, Z. Turbidity estimation from GOCI satellite data in the turbid estuaries of China's coast. *Remote Sens.* **2020**, *12*, 3770. [[CrossRef](#)]
31. Yin, W.; Huang, D. Applications of geostationary satellite data in the study of ocean and coastal short-term processes: Two cases in the East China Sea. In *Remote Sensing of Ocean and Coastal Environments*; Rani, M., Seenipandi, K., Rehman, S., Kumar, P., Sajjad, H., Eds.; Elsevier: Amsterdam, The Netherlands, 2020; pp. 139–154. ISBN 978-0-12-819604-5.
32. Cao, F.; Dai, K.; Tao, Q.; Fan, C.; He, L. Analysis of pollution status and research on treatment countermeasures in the coastal waters of Hangzhou Bay area. *Environ. Sci. Technol.* **2020**, *43*, 60–69. (In Chinese)
33. Wu, M.; Xu, J.; Feng, Y. Spatial and temporal distribution of sediment content in the mouth of Hangzhou Bay. *J. Sediment Res.* **2011**, *1*, 33–37. (In Chinese)
34. Lu, S.; He, M.; He, S.; He, S.Y.; Pan, Y.; Yin, W.; Li, P. An improved cloud masking method for GOCI data over turbid coastal waters. *Remote Sens.* **2021**, *13*, 2722. [[CrossRef](#)]
35. Nordkvist, K.; Loisel, H.; Gaurier, L.D. Cloud masking of SeaWiFS images over coastal waters using spectral variability. *Opt. Express* **2009**, *17*, 12246–12258. [[CrossRef](#)] [[PubMed](#)]
36. He, X.; Bai, Y.; Pan, D.; Huang, N.; Dong, X.; Chen, J.; Chen, C.A.; Cui, Q. Using geostationary satellite ocean color data to map the diurnal dynamics of suspended particulate matter in coastal waters. *Remote Sens. Environ.* **2013**, *133*, 225–239. [[CrossRef](#)]
37. Han, Z.; Yun, C.; Jiang, X. Experimental study on reflection spectral characteristics of suspended sediment. *J. Hydraul. Eng.* **2003**, *34*, 118–122. (In Chinese)
38. Von Luxburg, U. A tutorial on spectral clustering. *Stat. Comput.* **2007**, *17*, 395–416. [[CrossRef](#)]
39. Shi, J.; Malik, J. Normalized cuts and image segmentation. *IEEE Trans. Pattern Anal.* **2000**, *22*, 888–905. [[CrossRef](#)]

40. Hao, Q.; Chai, F.; Xiu, P.; Bai, Y.; Chen, J.; Liu, C.; Le, F.; Zhou, F. Spatial and temporal variation in chlorophyll a concentration in the Eastern China Seas based on a locally modified satellite dataset. *Estuar. Coast. Shelf Sci.* **2019**, *220*, 220–231. [[CrossRef](#)]
41. Hooker, S.B.; Esaias, W.E.; Feldman, G.C.; Gregg, W.W.; McClain, C.R. *An Overview of SeaWiFS and Ocean Color*; NASA Goddard Space Flight Center: Greenbelt, MD, USA, 1992.
42. Zhang, Y.; Ding, Y.; Li, T.; Xue, B.; Guo, Y. Seasonal variation of chlorophyll a and primary productivity in the East China Sea. *Oceanol. et Limnol. Sin.* **2016**, *47*, 261–268. (In Chinese)
43. Shen, X.; Hu, F. Basic characteristics of chlorophyll a distribution in the waters outside the Yangtze Estuary. *J. Fish. Sci. China* **1995**, *2*, 71–80. (In Chinese)
44. Wang, Y.; Chen, J.; Zhou, F.; Zhang, W.; Hao, Q. Spatial and temporal variations of chlorophyll a and primary productivity in the Hangzhou Bay. *J. Mar. Sci. Eng.* **2022**, *10*, 356. [[CrossRef](#)]
45. Cai, L.; Yu, M.; Yan, X.; Zhou, Y.; Chen, S. HY-1C/D reveals the chlorophyll-a concentration distribution details in the intensive islands' waters and its consistency with the distribution of fish spawning ground. *Remote Sens.* **2022**, *14*, 4270. [[CrossRef](#)]
46. Sha, H.; Li, X.; Yang, W.; Li, J. Inversion of interannual changes of sea surface temperature and chlorophyll a concentration from MODIS remote sensing data in the East China Sea. *J. Dalian Fish. Univ.* **2009**, *24*, 151–156. (In Chinese)
47. Chen, J.; Zhang, M.; Cui, T.; Wen, Z. A review of some important technical problems in respect of satellite remote sensing of chlorophyll-a concentration in coastal waters. *IEEE J. Sel. Top. Appl. Earth Obs. Remote Sens.* **2013**, *6*, 2275–2289. [[CrossRef](#)]
48. Ning, X.; Liu, Z. Assessment of primary productivity and potential fishery productivity in the Bohai, Yellow and East China Seas. *Acta Oceanol. Sin.* **1995**, *17*, 72–84. (In Chinese)
49. Zhang, J.; Shen, F.; Yu, X.; Zhou, Y. Winter and summer variation of phytoplankton absorption in the adjacent waters of Hangzhou Bay. *Geogr. Geo-Inf. Sci.* **2013**, *29*, 116–122. (In Chinese)
50. Shu, X.; Yin, Q.; Kuang, D. Relationship between chlorophyll concentration and reflection spectral characteristics of algae in inland water. *J. Remote Sens.* **2000**, *4*, 41–45. (In Chinese)
51. Han, L.; Rundquist, D.C.; Liu, L.L.; Fraser, R.N.; Schalles, J.F. The spectral responses of algal chlorophyll in water with varying levels of suspended sediment. *Int. J. Remote Sens.* **1994**, *15*, 3707–3718. [[CrossRef](#)]

Disclaimer/Publisher's Note: The statements, opinions and data contained in all publications are solely those of the individual author(s) and contributor(s) and not of MDPI and/or the editor(s). MDPI and/or the editor(s) disclaim responsibility for any injury to people or property resulting from any ideas, methods, instructions or products referred to in the content.